ORIGINAL ARTICLE

Journal
of the American Ceramic Society

# Experimental synthesis and density functional theory investigation of radiation tolerance of $Zr_3(Al_{1-x}Si_x)C_2$ MAX phases

Eugenio Zapata-Solvas[1] | Stavros-Richard G. Christopoulos[2] | Na Ni[1] | David C. Parfitt[2] | Denis Horlait[1,3] | Michael E. Fitzpatrick[2] | Alexander Chroneos[1,2] | William E. Lee[1]

[1]Centre for Nuclear Engineering (CNE) & Department of Materials, Imperial College London, London, UK

[2]Faculty of Engineering, Environment and Computing, Coventry University, Coventry, UK

[3]CNRS/IN2P3 and University of Bordeaux, Centre d'Etudes Nucléaires de Bordeaux-Gradignan, UMR 5797, Gradignan, France

**Correspondence**
Experimental
Eugenio Zapata-Solvas, Centre for Nuclear Engineering (CNE) & Department of Materials, Imperial College London, London, UK.
Email: Eugenio.zapata-solvas@imperial.ac.uk
DFT
Alexander Chroneos, Faculty of Engineering, Environment and Computing, Coventry University, Coventry, UK.
Email: Alexander.chroneos@imperial.ac.uk

**Abstract**

Synthesis, characterization and density functional theory calculations have been combined to examine the formation of the $Zr_3(Al_{1-x}Si_x)C_2$ quaternary MAX phases and the intrinsic defect processes in $Zr_3AlC_2$ and $Zr_3SiC_2$. The MAX phase family is extended by demonstrating that $Zr_3(Al_{1-x}Si_x)C_2$, and particularly compositions with $x \approx 0.1$, can be formed leading here to a yield of 59 wt%. It has been found that $Zr_3AlC_2$ - and by extension $Zr_3(Al_{1-x}Si_x)C_2$ - formation rates benefit from the presence of traces of Si in the reactant mix, presumably through the in situ formation of $Zr_ySi_z$ phase(s) acting as a nucleation substrate for the MAX phase. To investigate the radiation tolerance of $Zr_3(Al_{1-x}Si_x)C_2$, we have also considered the intrinsic defect properties of the end-members. $A$-element Frenkel reaction for both $Zr_3AlC_2$ (1.71 eV) and $Zr_3SiC_2$ (1.41 eV) phases are the lowest energy defect reactions. For comparison we consider the defect processes in $Ti_3AlC_2$ and $Ti_3SiC_2$ phases. It is concluded that $Zr_3AlC_2$ and $Ti_3AlC_2$ MAX phases are more radiation tolerant than $Zr_3SiC_2$ and $Ti_3SiC_2$, respectively. Their applicability as cladding materials for nuclear fuel is discussed.

**KEYWORDS**
density functional theory, MAX phases, powder synthesis, silicon

## 1 | INTRODUCTION

Although they were initially studied in the 1960s,[1] interest in the $M_{n+1}AX_n$ phases ($n$=integer, $M$=early transition metal; $A$=group 13-16 element and $X$=C or N) was regenerated by the report on the remarkable properties of $Ti_3SiC_2$ nearly two decades ago.[2] This was followed by the synthesis of numerous ternary[3] or quaternary solid solution MAX phases,[4,5] which also shared these metallic and ceramic properties (high elastic stiffness, high melting temperature, high thermal shock resistance, good machinability, high thermal, and electrical conductivity).[2,6-12] Such properties drive their technological importance and are attributed to their structure, which consists of the stacking of $n$ "ceramic" layer(s) interleaved by an $A$ "metallic" layer.[2,6-8]

MAX phases crystallize with the hexagonal $P6_3/mmc$ space group (no. 194).[1,2] The MAX phase family has three main forms, first $M_2AX$ (ie, $n$=1) type which are commonly

M-2 layer
X layer
M-1 layer

A layer

M-1 layer
X layer
M-2 layer

X layer
M-1 layer
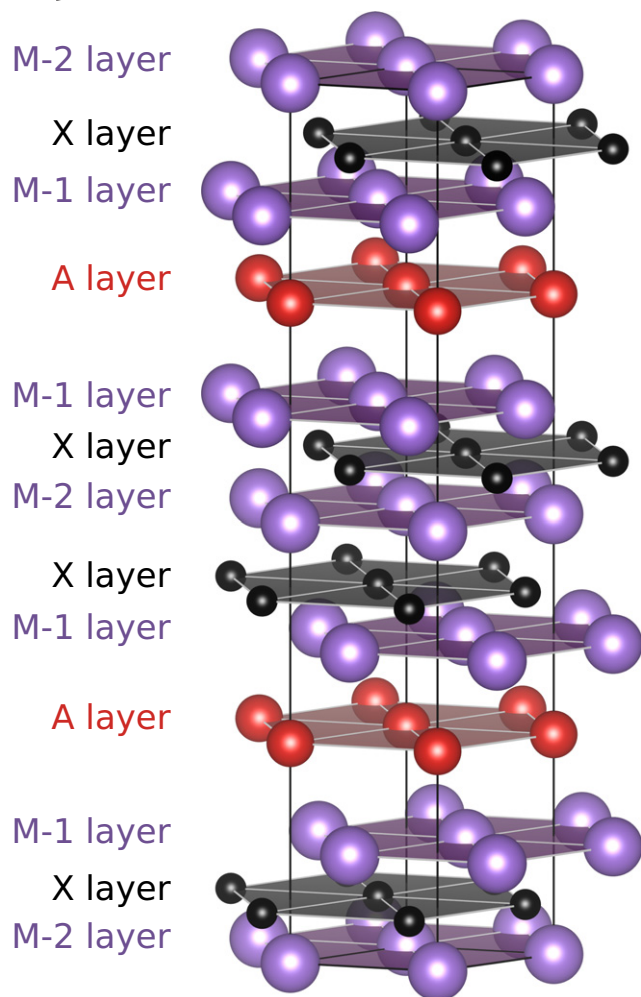
A layer

M-1 layer
X layer
M-2 layer

**FIGURE 1** Crystal structure of the $M_3AX_2$ phases with the $P6_3/mmc$ space group

referred as the 211 MAX phases, whereas the second type ($n=2$) are known as the 312 MAX phases, whereas the third type ($n=3$) are known as the 413 MAX phases. The 312 MAX phases are the subject of the present report. As illustrated in Figure 1, MAX phases possess a highly symmetric unit cell with atomic layers stacked along the c-direction.[1,2] For the 312 MAX phases, 3 $M$ layers sandwich 2 $X$ layers and form an $M_3X_2$ slab (with a face-centered-cubic-type stacking sequence), whereas $A$ layers separate these $M_3X_2$ slabs. The stacking around the $A$ layers has an HCP pattern and the $A$ layers form a mirror plane in the crystal.

As of today, the number of synthesized ternary MAX phases reaches almost 80 individual compounds;[3,9] and a fast-growing number of quaternary compounds that are sought for diverse reasons: tailoring certain physical properties (eg, an isotropic thermal expansion as obtained by Cabioch et al. for $Cr_2Al_{0.75}Ge_{0.25}C$),[13] triggering magnetic properties,[14] integrating an element not found in ternary MAX phases systems[5,15,16] or approaching as close as possible to a ternary

compound for which former synthesis attempts failed.[5,16] The latter reason motivated our research of synthesizing quaternary MAX phases with compositions as close as possible to the long-sought $Zr_2AlC$ and $Zr_3AlC_2$. Indeed, noting the absence of experimental reports of any Zr-Al-C-based ternary MAX phase and after failing with several $Zr_2AlC$ and $Zr_3AlC_2$ synthesis attempts, we turned to quaternaries and successfully produced several $Zr_2(Al_xA_{1-x})C$ compounds (with $A$=Sn, Sb, Pb, and Bi). This was before the Lapauw et al. reports in 2016 of both $Zr_2AlC$ and $Zr_3AlC_2$ successful syntheses[6,10] thereby making two important additions to the MAX phase family. The present report proposes an explanation on why they succeeded while other attempts failed. These long-sought compounds[5] are expected to display properties that can be of great interest and beneficial for several industrial applications, notably in the nuclear power field. A particular aim for Zr-Al-C materials is their application in Accident-Tolerant Fuels (ATF) via the deposition of a coating onto the exterior face of the Zr-based alloys commonly used as nuclear fuel cladding materials.[6,12,16-18] Such a coating would passively protect the cladding in severe accident conditions to avoid, or delay for several tens of hours, the rapid oxidation occurring at temperatures over 1200°C and associated production of hydrogen (as occurred at Fukushima).

The drive to consider a Zr-based MAX phase stems from the perceived compatibility that this material is expected to have with the Zr-based cladding material. Another great advantage of using Zr-based materials in nuclear fuel assembly components is the low neutron cross sections of the natural Zr isotopes that will not degrade reactor performance and cost-effectiveness. Coupled with the Zr nuclear properties, an element capable of diffusing rapidly to initiate a passivating outer oxide layer should also be present to provide the required high-temperature oxidation resistance. As such, Al, and to a lesser extent Si, are natural choices as they are known to be the better enhancers for high-temperature oxidation resistance of MAX phases[3] through the formation of $Al_2O_3$ and $SiO_2$ passivating scales, respectively.

The aim of this study was to synthesize $Zr_3AlC_2$ as well as quaternary solid solution $Zr_3(Al_{1-x}Si_x)C_2$ MAX phases. Trying to add Si to $Zr_3AlC_2$ was decided on the basis of the numerous reports on the analogous $Ti_3(Al_{1-x}Si_x)C_2$ system for which general increases of yield and purity of $Ti_3AlC_2$ were found when little Si was added to the reaction mix,[19-21] whereas maintaining the advantageous features of $Ti_3AlC_2$ such as oxidation resistance.[22,23]

Density functional theory (DFT) calculations were also employed to investigate the intrinsic defect processes of $Zr_3AlC_2$ and $Zr_3SiC_2$ to anticipate their behavior in high-irradiation environments. For comparison purposes, the latter work was extended to Ti-based analogues ($Ti_3AlC_2$ and $Ti_3SiC_2$), which are also considered for the ATF application.[11]

## 2 | METHODS

### 2.1 | Experimental methods

Commercial reactants used were $ZrH_2$ (APS 2-4 μm, >99.7%, grade S, Rockwood Lithium, Frankfurt, Germany), Al (-325 mesh, >99.9%, Alfa Aesar, Lancashire, UK), Si (-325 mesh, >99.9%, Alfa Aesar, UK), and C (>99.9%, Sigma Aldrich, Dorset, UK). Elemental mixtures for $Zr_3(Al_{1-x}Si_x)C_2$ were prepared with x=0, 0.1, 0.3, and 0.5. Stoichiometries for the 312 phase were adjusted to 3/1.1/1.0/1.9 for Zr/Al/Si/C to compensate for partial Al sublimation and C uptake from graphite crucibles during synthesis,[11] as usually reported in the MAX phase literature. The $Zr_3SiC_2$ end-member was not studied as solid solutions are energetically more favorable phases. Solid solutions were calculated to be formed as shown in different DFT studies, in which the enthalpy of mixing in $Ti_3(Al_{1-x},A_x)C_2$, $Ti_2(Al_{1-x},A_x)C$, and $Zr_2(Al_{1-x},A_x)C$ for different A elements, including Si, were calculated.[24] A glove box was used to avoid oxygen contamination or exposure to any hazardous process during handling. $Zr_3(Al_{1-x}Si_x)C_2$ precursor powders were ball milled for 30 minutes at 150 rpm in a nylon jar in a dry media using $ZrO_2$ balls in a planetary ball miller PM100 (Retsch, Han, Germany). Synthesis thermal treatments to precursors powders were carried out in graphite crucibles lined and capped with graphite film in a hot-press furnace HP W/25/1 (FCT, Rauenstein, Germany) at 1500°C for 1 hour under Ar atmosphere, according to the experimental conditions described by Lapauw et al.[10] for $Zr_3AlC_2$ synthesis. Note that pressure was not applied and powders were obtained after thermal treatments rather than dense billets. Synthesized powders were ground in an agate mortar with a pestle for X-ray diffraction (XRD) studies. A PANalytical instrument was used for XRD studies, using a 0.02° 2θ step and an angular range from 5 to 100°. Crystalline phase determination was carried out using the International Center for Diffraction Data database (ICDD) and the Xpert High Score plus software (PANalytical, Almelo, the Netherlands) for phase matching. Determination of lattice parameters was carried out using a full-pattern matching method (Le Bail function) with the help of the Fullprof suite program.[25] Xpert High Score software was also used to perform Rietveld refinements to obtain phase weight ratios starting with the unit cell parameters determined from the previous refinement methods. In all cases the differences in unit cell parameters between the two methods were found to be far below the values of associated uncertainties. Powders after thermal treatment were crushed in an agate mortar with a pestle and subsequently sieved up to a mesh of 320. Then, they were placed on an aluminum stub and coated with Cr to avoid charging effects during scanning electron microscope (SEM) observations. In addition, powder observations were carried out in a SEM Auriga (Zeiss, Oberkochen, Germany), under back-scattering electron (BSE) and secondary electron (SE) imaging modes, equipped with an energy-dispersive spectroscopy (EDS) detector with ultra-thin polymer window (Oxford Instruments, Oxford, UK). Transmission electron microscopy (TEM) of the synthesized powder was carried out in an aberration-corrected FEI Titan 80-300 S/TEM operated at 300 kV, equipped with a windowless energy dispersive X-ray spectroscopy (EDX) detector (Bruker QUANTAX 400-STEM, Bruker Corporation, Billerica, MA). As the Si K line is very close to the Zr L lines in the EDX spectrum, the background and peak fitting parameters were optimized using the Bruker Esprit EDX software and kept the same for all the quantification analysis to detect the potential presence of small contents of Si in some phases. The procedure yielded zero content of Si in undoped material, suggesting that the quantification is reasonably reliable for the comparison of Si contents.

### 2.2 | Computational methods

In this study, we employed the plane wave DFT code CASTEP.[26,27] Exchange and correlation interactions were formulated with the corrected density functional of Perdew, Burke and Ernzerhof (PBE)[28] within the generalized gradient approximation (GGA) and in conjunction with ultrasoft pseudopotentials.[29] The plane wave basis set was set to a cut-off of 450 eV, whereas a $3 \times 3 \times 1$ Monkhorst-Pack (MP)[30] k-point grid was used with a 108-atomic site supercell. All the calculations were under constant pressure conditions. We performed an extensive search to calculate the energetically favorable interstitials.
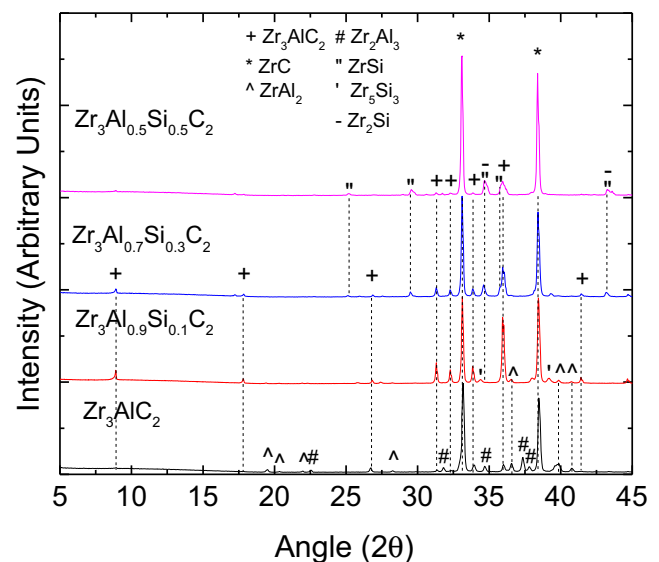


**FIGURE 2** X-ray diffractograms of Zr3(Al1-xSix)C2 with Si/(Si + Al)=0, 0.1, 0.3, 0.5

# 3 | RESULTS AND DISCUSSION

## 3.1 | Synthesis and characterization of $Zr_3(Al_{1-x}Si_x)C_2$ MAX phase

Crystalline phase determination by XRD is shown in Figure 2. It first reveals the formation of a 312 MAX phase in the four samples along with ZrC. The refinement results are reported in Table 1. The lattice parameters for the 312 MAX phases were all close to those determined by Lapauw et al.[10,11] for $Zr_3AlC_2$. From this and subsequent characterizations detailed thereafter, it is reasonable to assume that $Zr_3(Al_{1-x}Si_x)C_2$ compositions were formed. In addition, the lattice parameters refined for the ZrC phases are similar in the first three samples and are equal to the lowest reported ones for $ZrC_{1-x}$ (even in Si free synthesis), which suggests that highly substoichiometric $ZrC_{1-x}$ is formed with $x \approx 0.4$.[31] From Rietveld refinements, when $Si/(Si + Al)=0$, $Zr_3AlC_2$ is present as a residual phase (7 wt%) (Table 1). However, the formation of $Zr_3AlC_2$ or $Zr_3(Al_{1-x}Si_x)C_2$ is greatly promoted by the addition to the reaction mix of Si for $Si/(Si + Al)=0.1$ (59 wt%) and $Si/(Si + Al)=0.3$ (47 wt%). The yield, however, decreases greatly for $Si/(Si + Al)=0.5$ (11 wt%).

In all samples with Si, a minor Si-based phase is found ($Zr_5Si_3$ for $Si/(Si + Al)=0.1$, $Zr_2Si$ for $Si/(Si + Al)=0.3$ and 0.5 and ZrSi for $Si/(Si + Al)=0.5$) and this therefore suggests that the solubility of Si in $Zr_3(Al_{1-x}Si_x)C_2$ may be limited ($x<0.1$) or that Si incorporation in $Zr_3(Al_{1-x}Si_x)C_2$ is kinetically hindered under the present synthesis conditions.

When the $a$ and $c$ lattice parameters of the obtained MAX phases are compared (Table 1), an increase in $a$ with the $Si/(Al + Si)$ starting ratio and conversely a decrease in $c$ (and of the cell volume) are observed (we exclude the value obtained for $Si/(Si + Al)=0.5$ as the uncertainty is too high). Interestingly, the relative changes are greater between $Si/(Si + Al)=0$ vs $Si/(Si + Al)=0.1$ than between $Si/(Si + Al)=0.3$ vs $Si/(Si + Al)=0.1$ (eg, $a_{0.1}=1.0013$ $a_0$ while $a_{0.3}=1.0004$ $a_{0.1}$). This further suggests that Si incorporation in $Zr_3(Al_{1-x}Si_x)C_2$ should be limited and should saturate close to $x=0.1$ (at least for our selected experimental conditions).

Scanning Electron Microscopy (SEM) observations of synthesized powders (Figure 3) confirmed the greater formation of a 312 MAX phase for $Si/(Si + Al)=0.1$ or 0.3 compared to $Si/(Si + Al)=0$ or 0.5. The compositions with the lowest and highest 312 MAX phase content, $Si/(Si + Al)=0$ and $Si/(Si + Al)=0.1$, respectively, are shown in Figure 3 to illustrate the different aspect ratios of the ZrC and 312 MAX phases. Numerous layered particles were observed in $Zr_3(Al_{1-x}Si_x)C_2$ for $Si/(Si + Al)=0.1$, suggesting the predominance of layered $Zr_3(Al_{1-x}Si_x)C_2$ MAX phase, whereas for $Si/(Si + Al)=0$ the particles were predominantly equiaxed with a size of ~2 μm. A clearer example of the characteristic MAX phase grain laminar microstructure is shown in Figure 4. EDX measurements (Figure 4) were performed firstly to confirm formation of $Zr_3AlC_2$ and $Zr_3(Al_{1-x}Si_x)C_2$ MAX phases notably through measurement of the $Zr/(Al + Si)$ ratio, which was determined, as expected, to be equal or close to 3. EDX investigations also revealed that in the $Si/(Si + Al)=0.1$ and $Si/(Si + Al)=0.3$ samples the MAX phase grains had variable Si contents (Figure 4): some grains were even found free of Si (in the limits of sensitivity of the detector, being less

**TABLE 1** Summary of synthesis results of the $Zr_3(Al_{1-x}Si_x)C_2$ MAX phase

| Targeted compound | Phases | Structure | a (Å) | b (Å) | c (Å) | V (Å³) | Volume ratio (%) |
|---|---|---|---|---|---|---|---|
| $Zr_3AlC_2$ | $Zr_3AlC_2$ | $P6_3/mmc$ | 3.3287 (4) | 3.3287 (4) | 20.011 (1) | 192.01 (6) | 7 ± 1 |
| | ZrC | Fm-3 m | 4.6866 (2) | 4.6866 (2) | 4.6866 (2) | 102.94 (2) | 66 ± 2 |
| | $ZrAl_2$ | $P6_3/mmc$ | 5.2856 (9) | 5.2856 (9) | 8.754 (2) | 211.8 (1) | 8 ± 1 |
| | $Zr_2Al_3$ | Fdd2 | 5.5693 (7) | 9.533 (6) | 13.90 (1) | 738 (1) | 19 ± 1 |
| $Zr_3(Al_{0.9}Si_{0.1})C_2$ | $Zr_3AlC_2$ | $P6_3/mmc$ | 3.3331 (2) | 3.3331 (2) | 19.940 (1) | 191.85 (4) | 59 ± 2 |
| | ZrC | Fm-3 m | 4.6834 (2) | 4.6834 (2) | 4.6834 (2) | 102.72 (2) | 31 ± 2 |
| | $ZrAl_2$ | $P6_3/mmc$ | 5.287 (2) | 5.287 (2) | 8.744 (4) | 211.7 (2) | 5 ± 1 |
| | $Zr_5Si_3$ | $P6_3/mmc$ | 7.965 (2) | 7.965 (2) | 5.502 (6) | 302.3 (5) | 5 ± 1 |
| $Zr_3(Al_{0.7}Si_{0.3})C_2$ | $Zr_3AlC_2$ | $P6_3/mmc$ | 3.3344 (3) | 3.3344 (3) | 19.914 (2) | 191.75 (6) | 47 ± 2 |
| | ZrC | Fm-3 m | 4.6871 (2) | 4.6871 (2) | 4.6871 (2) | 102.97 (2) | 47 ± 2 |
| | $Zr_2Si$ | I4/mmc | 6.624 (2) | 6.624 (2) | 5.349 (7) | 235.3 (5) | 6 ± 1 |
| $Zr_3(Al_{0.5}Si_{0.5})C_2$ | $Zr_3AlC_2$ | $P6_3/mmc$ | 3.31 (3) | 3.31 (3) | 20.2 (3) | 192 (1) | 12 ± 2 |
| | ZrC | Fm-3 m | 4.6914 (5) | 4.6914 (5) | 4.6914 (5) | 103.25 (9) | 76 ± 2 |
| | $Zr_2Si$ | I4/mmc | 6.618 (3) | 6.618 (3) | 5.356 (5) | 234.6 (4) | 11.5 ± 2 |
| | ZrSi | Pnma | 7.11 (2) | 3.723 (7) | 5.18 (2) | 137 (1) | 0.5 ± 1 |
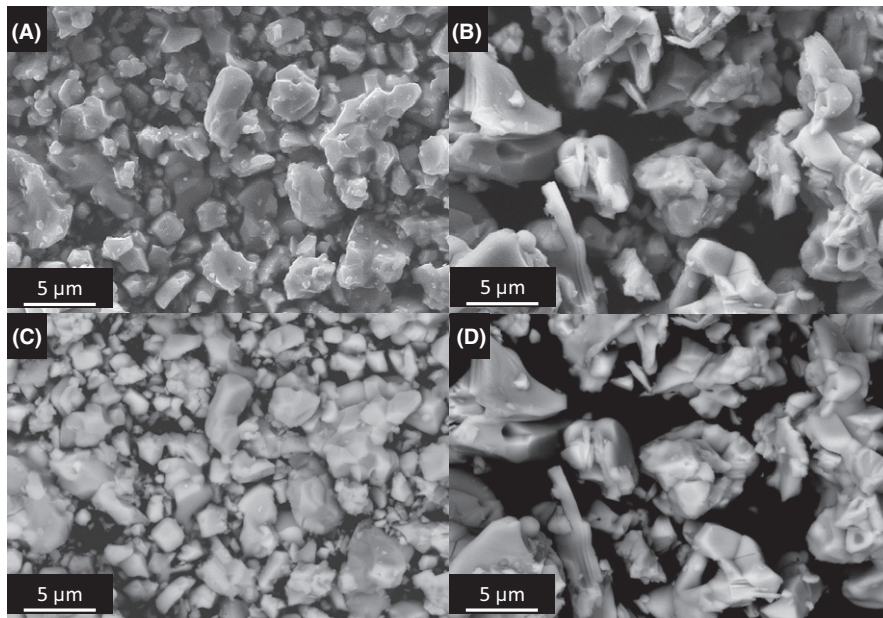
**FIGURE 3** SEM images: Secondary electron images (A) $Zr_3AlC_2$ and (B) $Zr_3(Al_{0.9}Si_{0.1})C_2$ and their respective back scattered electron images (C) and (D)
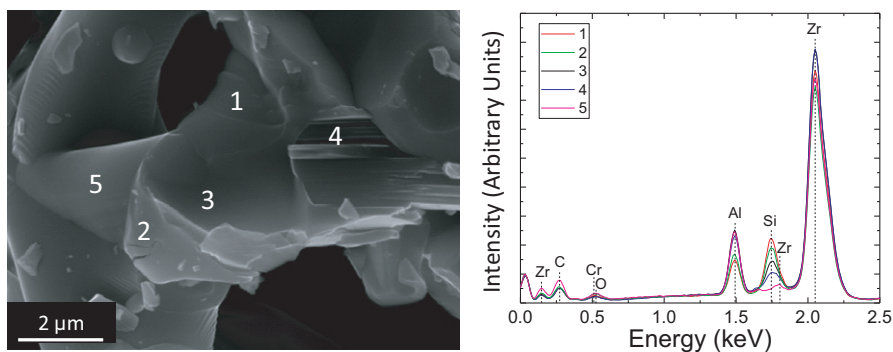


**FIGURE 4** SEM image (SE) on left with EDX point analysis of numbered regions on right. The lower the number of the EDX spot, the higher the Si content

than 1 at.%). Interestingly, changes in Si content were balanced by Al content, confirming the occurrence of partial substitution of Al by Si in $Zr_3AlC_2$. The only possible reason for the variable content of Si in $Zr_3AlC_2$ is that Si incorporation in $Zr_3(Al_{1-x}Si_x)C_2$ was subsequent to $Zr_3AlC_2$ formation and that the diffusion/substitution rate was too slow at the reaction temperature to achieve complete and homogeneous Si distribution within 1 hour (the Si content in a MAX grain being therefore correlated with the quantity of the Si-rich grains touching this MAX grain during the synthesis). Further investigations are presented in what follows to confirm this hypothesis. Based on EDX results, it was unclear whether the $Zr_3AlC_2$ grains contain O or not, as the samples were coated with Cr for SEM observations and the O peak in EDX is overlapped by one of the Cr peaks as can be observed in Figure 4.

TEM investigation of the presence of oxygen in the synthesized powders was done for the $Zr_3(Al_{0.9}Si_{0.1})C_2$ and $Zr_3AlC_2$ target samples only (Figures 5 and 6). The bright-field TEM of the $Zr_3(Al_{0.9}Si_{0.1})C_2$ sample given in Figure 5 shows different particles of two phases: $Zr_3AlC_2$ and $Zr_5Si_3$. $Zr_5Si_3$ shows Al content as high as 20 at.%, suggesting solid solubility of Al in $Zr_5Si_3$, although it is noted that the quantified content can only be taken as an indication since the result was not calibrated with standards. In addition, these particles contain minor amounts of C and O, up to a maximum of 3 and 2 at.%, respectively. However, the $Zr_3AlC_2$ phase also contains some minor amounts of Si, which is clearly shown by a comparison of the EDX spectra obtained from the $Zr_3(Al_{0.9}Si_{0.1})C_2$ and the undoped $Zr_3AlC_2$ samples (Figure 5). Qualitative compositional analyses suggested a Si content of as high as ~1.7 at.% (x=0.102 assuming that the Al + Si content is 1/6), in agreement with the maximum solubility of Si in the targeted $Zr_3(Al_{1-x}Si_x)C_2$ phase as suggested by lattice parameters calculated from XRD results in Table 1. It
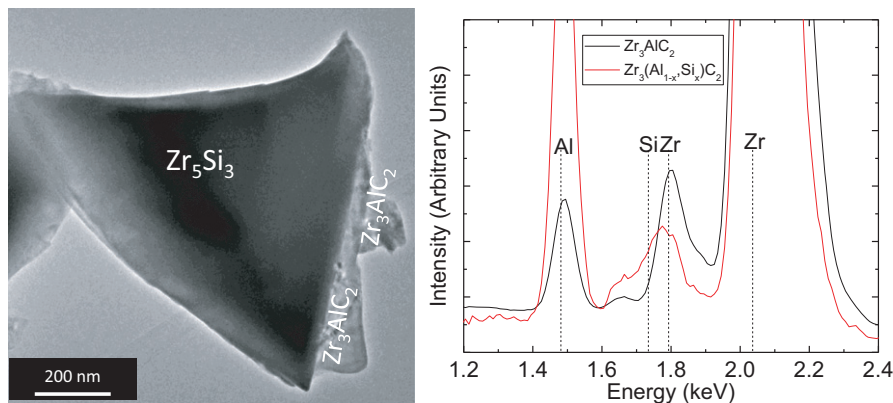
**FIGURE 5** Bright-field TEM image of the $Zr_3(Al_{0.9}Si_{0.1})C_2$ sample on left with right an EDX spectrum for a $Zr_3AlC_2$ grain containing Si. The EDX spectrum of the $Zr_3AlC_2$ sample that does not contain Si (as shown in Figure 6) is included here for comparison

is also noteworthy that the previously reported Si solubility in other Zr-Al-C-based ternary laminar carbides at a similar level: for example, maximum solubilities of $(ZrC)_m[Al_{1-z}Si_z]_8C_6$ and $(ZrC)_m[Al_{1-z}Si_z]_4C_3$ are 0.07 and 0.11, respectively.[32,33] In addition, no Si was detected in all $Zr_3AlC_2$ grains studied in the composition without Si, which confirms that Si is not a major impurity in the $ZrH_2$, Al or C powders (Table 2). STEM-EDX also revealed the presence of O in the $Zr_3(Al_{1-x}Si_x)C_2$ phase, indicating the partial oxidation of the powders during processing. Figure 6 illustrates an average $Zr_3AlC_2$ particle on synthesized powders for Si/(Si + Al)=0.1

The source of O is not clear but it could come either from: (i) contamination with the $ZrO_2$ milling media used to homogeneously mix the elemental precursors, although the speed of 150 rpm used in this study compared to the

400 rpm conventionally used to mill[5] or mix ceramic powders is as low as possible to minimize contamination but high enough to produce homogeneous mixing; (ii) exposure of powders to air prior to and after synthesis; (iii) TEM sample preparation (samples were prepared by inserting the grid in the powders a couple of times without any extra procedures which makes this step highly unlikely to introduce any O). Considering the total content of O and C of different particles measured, the stoichiometry correlates well with the total C expected to be present, which suggests a generic $Zr_3(Al_{1-x}Si_x)(C_{1-y}O_y)_2$ phase formation, consistent with the observed Zr, Al:Si, C:O stoichiometry of 3:1:2. O does not belong to the family of MAX phases, however, previous studies have reported oxygen substituting for C in $Ti_2AlC$ at levels as high as 12.5 at.% which correlates with 50% of C substitution.[34-37]

**TABLE 2** Elemental contents (wt%), including impurities, according to Rockwood lithium, which is the $ZrH_2$ supplier of Chemetall

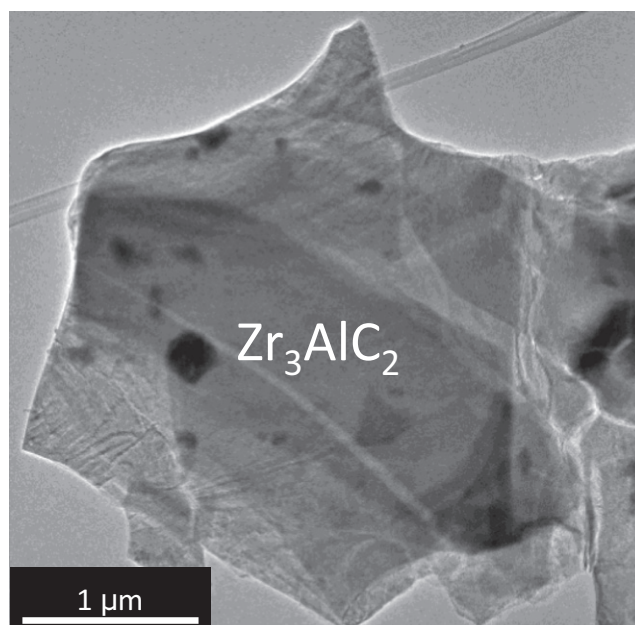| Element content | Grade G (Lapauw et al.)[6,10] | Grade S (This work) |
|---|---|---|
| Zr + Hf | 97.6 ± 0.5% | 97.2 ± 0.5% |
| Hf | approx. 2% | min. 0.2% |
| H | min. 1.9% | min. 1.9% |
| Si | max. 0.5% | max. 0.1% |
| Fe | max. 0.08% | max. 0.1% |
| Cl | max. 0.05% | max. 0.02% |
| Al | max. 0.3% | – |
| Ti | max. 0.3% | – |
| Mg | max. 0.2% | – |
| Cr | – | max. 0.1% |
| Ca total | max. 0.15% | – |
| Ca soluble | max. 0.05% | – |



**FIGURE 6** Bright-field TEM image for a $Zr_3AlC_2$ grain

Defect enthalpy formation for O partial substitution has shown in $Ti_2AlC$ that the most likely position for the O to be located is substituting for C in the MX blocks of MAX phases.[38] However, the second lowest enthalpy for O partial substitution is for interstitial O in an Al layer at the center of a bi-triangular pyramid with M atoms at the vertex.[39] It has been experimentally observed in $Cr_2AlC$ that O is partially substituting for the Al,[40] which was also the most likely substitution observed in this system in the theoretical calculations mentioned earlier, but also limits its maximum content to 3.5 at.%.[39] Furthermore, it was predicted for $Zr_2AlC$ and $Hf_2AlC$ that O would partially substitute for C in the case that these phases could be experimentally synthesized. Therefore, our experimental observations qualitatively agree well with the prediction for the 211 $Zr_2AlC$ and it seems reasonable to suggest the formation of $Zr_3(Al_{1-x}Si_x)(C_{1-y}O_y)_2$. The presence of O may be undesirable but, if it comes from the milling media, as a result of a substitution reaction that stabilizes the MAX phase or as exposure of the powders in air either before being placed in the hot press or after synthesis, it is difficult to avoid. Also, carbothermal reduction processes require higher temperatures, above 1657°C in the case of $ZrO_2$,[34] and longer times to be completed, which would produce a complete degradation of any MAX phase structure. For example, it was previously reported that the reaction of $ZrO_2$ with C forms different $ZrC_xO_y$ particles under oxidation experiments at temperatures above 1500°C (the same temperature used in this work to produce the MAX phase).[41] Although the presence of O is undesirable, the $ZrC_xO_y$ particles stabilize the long-term oxidation behavior of $ZrB_2$-SiC composites.[41] Therefore, although being at first sight a detrimental feature, the inclusion of O in these materials may turn out to be beneficial: firstly as it probably stabilizes the structure and secondly because it could act as a reservoir for internal self-healing with shorter diffusion paths.[38] Further investigations are undergoing to locate O in the $Zr_3(Al_{1-x}Si_x)C_2$ structure.

When reporting for the first time the synthesis of the long-sought $Zr_2AlC$ and $Zr_3AlC_2$ MAX phases, Lapauw et al.[10] stated that "At this moment, it is not easy to explain the failure of others to synthesize this Zr-based MAX phase, which was produced readily and repeatedly in this work. One possible reason is the use of $ZrH_2$ raw powders, which might have facilitated the nucleation of these nanolayered carbides. The results of this work suggest that the key in synthesizing such complex phases is inextricably linked with their nucleation. These comments notwithstanding, it is hereby acknowledged that more work is required to identify the starting materials and processing conditions favoring the formation of the hitherto elusive $Zr_3AlC_2$ MAX phase". It was clear for us that $ZrH_2$ by itself could not be the key reason for successful synthesis of $Zr_2AlC$ and $Zr_3AlC_2$ since: (i) we did not succeed in forming $Zr_2AlC$[5] and obtained $Zr_3AlC_2$ with a low yield starting from $ZrH_2$; and (ii) $ZrH_2$ decomposes at only ~800°C and Zr presumably readily reacts with graphite to form ZrC, so that the actual precursor for MAX phase formation is ZrC. The findings of the present work, however, tend to confirm their hint that nucleation is the key to achieveing $Zr_3AlC_2$ (and presumably $Zr_2AlC$ and $Zr_3(Al_{1-x}Si_x)C_2$) synthesis. During TEM observations of the Si/(Si + Al)=0.1 reacted sample, it was noted that $Zr_5Si_3$ particles seem to have MAX phase particles attached to their boundaries (Figure 5), giving the impression that MAX grains are forming and growing out of $Zr_5Si_3$ grains. Such phenomena, the $Zr_3AlC_2$ particles collated to $Zr_5Si_3$ particles, was observed repeatedly throughout the $Zr_3(Al_{0.9}Si_{0.1})C_2$ powders. $Zr_5Si_3$ particles thus potentially serve as substrates for $Zr_3(Al_{1-x}Si_x)C_2$ nucleation and growth. This would imply that such heterogeneous nucleation processes provided by $Zr_5Si_3$ grains either strongly enhance the nucleation rate of $Zr_3(Al_{1-x}Si_x)C_2$ (so that formation rate of the MAX phase gets faster than its dissociation rate) or that, according to the Classical Nucleation Theory,[42] surface effects decrease sufficiently the barrier of the MAX phase free energy of nucleation so that nucleation becomes far more energetically favorable, which leads to an increased yield as high as 59 wt% for Si/(Si + Al)=0.1.

For the $Zr_3(Al_{0.7}Si_{0.3})C_2$ synthesis attempt, a high MAX phase content was also obtained although $Zr_5Si_3$ was not found by XRD at the end of the heat treatment. This, however, does not discredit the hypothesis presented here, since $Zr_2Si$ could have the same influence as $Zr_5Si_3$ (lowering $Zr_3AlC_2$ nucleation-free energy by surface effects) and/or $Zr_5Si_3$ could have transformed to $Zr_2Si$ after having served as a fertile ground for the MAX phase nucleation of Si (owing to the slow depletion of Si diffusing into the MAX phase): hence Si and/or $Zr_5Si_3$ may be present but remain undetected by XRD owing to low content and/or low crystallinity. To be conservative, we will, however, continue developing our hypothesis considering more generic $Zr_ySi_z$ phase(s). Table 2 shows the content of the different elements from the $ZrH_2$ source powders used in the reports of Lapauw et al.[6,10] and in the present work, according to the manufacturers' data. Notably, the major difference between the two commercial powders concerns Si maximum content: that of Lapauw et al. is ≤0.5 wt% and in this study it is ≤0.1 wt%. In molar content in the reaction mix for $Zr_3AlC_2$ synthesis these values correspond to maxima of about 0.83 and 0.17 mol%, respectively, which is to be compared to the 1.67 mol% of Si introduced for the $Zr_3(Al_{0.9}Si_{0.1})C_2$ synthesis attempt. It is therefore most likely that in both this study and that of Lapauw et al. during attempts to produce $Zr_3AlC_2$, the $Zr_ySi_z$ helped the nucleation and growth of $Zr_3AlC_2$. However, the attempt of Lapauw et al. led to an order of magnitude higher $Zr_3AlC_2$ yield thanks to the higher Si impurity level in their $ZrH_2$ powder batch. It is

notable that the $Zr_3AlC_2$ samples with no Si addition contain 7 wt% of $Zr_3AlC_2$, which could be related to the small content of Si ($\leq 0.1$ wt%) in the $ZrH_2$ source powders (Table 2).

Retrospectively, the suggested reaction mechanism may also explain the heterogeneous distribution evidenced by EDX of Si in the MAX phase grains. Indeed, it is likely that Si may diffuse from $Zr_ySi_z$ grains into the attached MAX phase grains while Al is moving in the opposite direction, in agreement with the notable Al content found in $Zr_5Si_3$ grains during the TEM investigation. This inter-diffusion would, however, proceed at a slower rate than that of MAX phase grain growth, so that Si is found heterogeneously (the closer to the $Zr_ySi_z$ substrate, the higher the Si content in the MAX phase).

In summary, our investigations and comparison to the Lapauw et al. results allowed the gathering of a body of corroborating evidence that Si impurities are likely to have a beneficial impact on $Zr_3AlC_2$ (and by extent on $Zr_3(Al_{1-x},Si_x)C_2$ and $Zr_2AlC$) nucleation and/or formation yields. A last indirectly converging proof comes from $Ti_3AlC_2$, where previous studies[19,20] observed that, all the other experimental parameters being the same, $Ti_3AlC_2$ yield, purity and grain size were greatly improved by the deliberate addition of Si ($\sim$1 to 4 at.%) in the reaction powder mix. Interestingly, Zhou et al.[21] even proved this allowed reducing the reaction temperature. Furthermore, Xu et al.[19] found residual traces of $Ti_5Si_3$ when synthesizing $Ti_3(Al_{1-x},Si_x)C_2$ solid solutions. This similarity between $Zr_3AlC_2$ and $Ti_3AlC_2$ syntheses in the presence of Si further suggests that silicides in general may help in forming and/or accelerate MAX phase formation and this could be a lead to follow to try synthesizing new MAX phases and/or to try improving their purity.

## 3.2 | DFT study of radiation tolerance

Radiation damage in essence is an accumulation of defects formed by displacement cascades.[11,43,44] Calculation of the energy of Frenkel defects is important for nuclear applications, as a low pair formation energy is associated with greater numbers of more persistent defects which in turn lead to a loss of the material's crystal structure. Relations 1-3 are the three key Frenkel reactions in Kröger-Vink notation (ie, $V_M$ and $M_i$ will denote a vacant M site and a M interstitial defect, respectively)[45]

$$M_M \rightarrow V_M + M_i \tag{1}$$
$$A_A \rightarrow V_A + A_i \tag{2}$$
$$X_X \rightarrow V_X + X_i \tag{3}$$
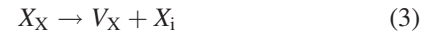
For all the MAX phases considered the energetically favorable interstitials are reported in Table 3.

During radiation damage, the point defects formed by the displacement cascade will either recombine or occupy an alternative lattice site forming an antisite defect.[11] The physical meaning of a low-energy antisite formation energy is that a large proportion of residual defects will remain in the material.[11,46] Relations 4-6 refer to the simple antisite formation mechanisms:

$$M_M + A_A \rightarrow M_A + A_M \tag{4}$$
$$M_M + X_X \rightarrow M_X + X_A \tag{5}$$
$$A_A + X_X \rightarrow A_X + X_A \tag{6}$$
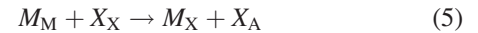
Interstitial defects preferentially form in the $A$ layer therefore their association with $V_A$ needs to be considered:

$$M_i + V_A \rightarrow M_A \tag{7}$$
$$X_i + V_A \rightarrow X_A \tag{8}$$

Relations 7 and 8 reveal whether $M_i$ and $X_i$ defects will recombine with $V_A$ to form $M_A$ and $X_A$ antisites, respectively, or remain as interstitials.

In addition, after displacement cascades the overstoichiometry of interstitials may lead to the displacement of atoms from their lattice sites to interstitial sites with the concurrent formation of antisite defects. For example, in $\gamma$-TiAl the following reaction may take place $Ti_i + Al_{Al} \rightarrow Ti_{Al} + Al_i$.[46] This leads to the reduction in the unfavorable $Ti_i$ and increases the concentration of $Ti_{Al} + Al_i$.[46] Equivalent reactions were examined in $Ti_3SiC_2$ and were deemed energetically unfavorable.[11] The following reactions will be considered here for completeness:

$$M_i + A_A \rightarrow M_A + A_i \tag{9}$$
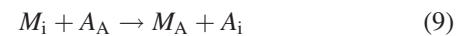
## 3.3 | Trends and implications of defect processes

An assessment of the radiation performance of materials is their propensity to form and accommodate point defects.[44]

**TABLE 3** Positions of the energetically favourable interstitials for the 312 MAX phases considered

| | M | A | X |
|---|---|---|---|
| $Zr_3SiC_2$ | 0.77832, 0.84054, 0.25082 | 0.55056, 0.27774, 0.25086 | 0.33333, 0.66669, 0.25073 |
| $Zr_3AlC_2$ | 0.75939, 0.84831, 0.25150 | 0.66870, 0.33984, 0.25077 | 0.33333, 0.66669, 0.73437 |
| $Ti_3SiC_2$ | 0.75228, 0.70167, 0.25075 | 0.66381, 0.33063, 0.25073 | 0.33510, 0.66492, 0.24999 |
| $Ti_3AlC_2$ | 0.27651, 0.28686, 0.25068 | 0.66033, 0.33072, 0.25078 | 0.33588, 0.66414, 0.25002 |

This is because materials can be destabilized by the accumulation of defects, which can in turn lead to volume changes and microcracking.[44,47,48] A consequence of the displacive radiation is an athermal concentration of Frenkel pairs. The radiation tolerance of a material will be determined by the resistance to the formation of persistent populations of Frenkel (and antisite) defects, therefore a high defect energy is a factor of radiation tolerance.[44]

Previous experimental studies[49,50] determined that $Ti_3AlC_2$ is more tolerant to radiation damage compared to $Ti_3SiC_2$. For the analogous MAX phases $Zr_3AlC_2$ and $Zr_3SiC_2$ considered here there are limited synthesis results on $Zr_3AlC_2$ (Ref. 10) and $Zr_3(Al_{0.9}Si_{0.1})C_2$ (the present study) but no radiation damage studies. On the grounds of the defect processes investigated by DFT (Tables 4 and 5) it can be inferred that $Zr_3AlC_2$ will be more radiation tolerant than the hypothetical $Zr_3SiC_2$. This is because the lowest energy intrinsic disorder mechanism (relation 2, the Frenkel reaction) in $Zr_3AlC_2$ is higher in energy compared

to $Zr_3SiC_2$ (1.46 eV and 1.40 eV, respectively, refer to Table 5) and therefore there will be a lower concentration of Frenkel defects in $Zr_3AlC_2$. On these grounds, comparing with $Ti_3AlC_2$ and $Ti_3SiC_2$ it can be inferred that these Ti-based MAX phases have even higher Frenkel energies and therefore they can be superior in a radiation environment (Tables 4 and 5).

For $Zr_3AlC_2$ the Frenkel formation energy of Al is significantly lower compared to the Frenkel formation energy of Zr and C. This implies that the population of $Al_i$ and $V_{Al}$ will be higher than the other point defects. Interestingly, for $Zr_3AlC_2$ and $Zr_3SiC_2$ relation 9 is favorable by – 0.27 eV and –0.17 eV respectively (refer to Table 5). This indicates that there is a direct route to transform $Zr_i$ to $Zr_{Al}$ and $Al_i$ (and $Zr_i$ to $Zr_{Si}$ and $Si_i$ for $Zr_3SiC_2$). This is in contrast to that calculated for the Ti-based 312 MAX phases considered here where Relation 9 has positive energies (refer to Table 4). Although the kinetics of this process need to be considered in $Zr_3SiC_2$ it is noteworthy that the high mobility of $Si_i$ in the analogous $Ti_3SiC_2$ suggests a rapid recovery mechanism for $Si_i$.

A trend that was identified in all the 312 MAX phases considered here is that the $M_i$ preferentially fill a $V_A$ (relation 7), whereas the $C_i$ remains an interstitial (relation 8). This implies that $M_A$ antisite defects will exist after a displacement cascade; however, C is expected to either exist as an interstitial species or at its crystallographic site. Importantly, in the Ti-based MAX phases this process is significantly more favorable than in the Zr-based MAX phases. This implies that the concentration of $M_A$ antisites via this process will be more pronounced in the Ti-based MAX phases. This process will only be significant after irradiation given that the formation of the $M_i$ defects via the Frenkel reaction (relation 1) will be prohibitive owing to the high reaction energies for all the MAX phases considered here (6.12-7.32 eV, refer to Tables 4 and 5). In any case the radiation-damaged Ti-based MAX phases will more readily form $M_A$ antisite defects, reducing their $M_i$ and $V_A$ concentrations. The equivalent process for the formation of $X_A$ antisites (relation 8) is not energetically favorable for any of the MAX phases considered here (0.06-0.46 eV, refer to Tables 4 and 5). Nevertheless, given that $Zr_3AlC_2$ is likely to be more compatible to the Zr-alloy of the cladding it is a good candidate material for passive safety protection of nuclear fuel cladding. However, its radiation tolerance and oxidation resistance at high temperature will need to be determined.

Defect reactions can provide important information on the radiation tolerance of MAX phases. However, they should be verified by experiments and theoretical calculations of migration energy barriers and cascade processes.[51-56] The present results are consistent with previous DFT studies for $Ti_3AlC_2$ and $Ti_3SiC_2$ MAX phases.[11,53]

**TABLE 4** Calculated defect reaction energies (in eV, for relations 1-9) for $Ti_3AlC_2$ and $Ti_3SiC_2$

| Reaction | $Ti_3AlC_2$ | Reaction | $Ti_3SiC_2$ |
|---|---|---|---|
| $Ti_{Ti} \rightarrow V_{Ti} + Ti_i$ | 7.32 | $Ti_{Ti} \rightarrow V_{Ti} + Ti_i$ | 7.30 |
| $Al_{Al} \rightarrow V_{Al} + Al_i$ | 3.40 | $Si_{Si} \rightarrow V_{Si} + Si_i$ | 3.19 |
| $C_C \rightarrow V_C + C_i$ | 3.17 | $C_C \rightarrow V_C + C_i$ | 3.09 |
| $Ti_{Ti} + Al_{Al} \rightarrow Ti_{Al} + Al_{Ti}$ | 3.27 | $Ti_{Ti} + Si_{Si} \rightarrow Ti_{Si} + Si_{Ti}$ | 4.65 |
| $Ti_{Ti} + C_C \rightarrow Ti_C + C_{Ti}$ | 10.52 | $Ti_{Ti} + C_C \rightarrow Ti_C + C_{Ti}$ | 13.44 |
| $Al_{Al} + C_C \rightarrow Al_C + C_{Al}$ | 9.26 | $Si_{Si} + C_C \rightarrow Si_C + C_{Si}$ | 6.28 |
| $Ti_i + V_{Al} \rightarrow Ti_{Al}$ | -3.25 | $Ti_i + V_{Si} \rightarrow Ti_{Si}$ | −2.69 |
| $C_i + V_{Al} \rightarrow C_{Al}$ | 0.31 | $C_i + V_{Si} \rightarrow C_{Si}$ | 0.06 |
| $Ti_i + Al_{Al} \rightarrow Ti_{Al} + Al_i$ | 0.15 | $Ti_i + Si_{Si} \rightarrow Ti_{Si} + Si_i$ | 0.50 |

**TABLE 5** Calculated defect reaction energies (in eV, for relations 1-9) for $Zr_3AlC_2$ and $Zr_3SiC_2$

| Reaction | $Zr_3AlC_2$ | Reaction | $Zr_3SiC_2$ |
|---|---|---|---|
| $Zr_{Zr} \rightarrow V_{Zr} + Zr_i$ | 6.12 | $Zr_{Zr} \rightarrow V_{Zr} + Zr_i$ | 6.78 |
| $Al_{Al} \rightarrow V_{Al} + Al_i$ | 1.46 | $Si_{Si} \rightarrow V_{Si} + Si_i$ | 1.40 |
| $C_C \rightarrow V_C + C_i$ | 3.47 | $C_C \rightarrow V_C + C_i$ | 2.78 |
| $Zr_{Zr} + Al_{Al} \rightarrow Zr_{Al} + Al_{Zr}$ | 3.46 | $Zr_{Zr} + Si_{Si} \rightarrow Zr_{Si} + Si_{Zr}$ | 4.96 |
| $Zr_{Zr} + C_C \rightarrow Zr_C + C_{Zr}$ | 10.60 | $Zr_{Zr} + C_C \rightarrow Zr_C + C_{Zr}$ | 14.14 |
| $Al_{Al} + C_C \rightarrow Al_C + C_{Al}$ | 8.43 | $Si_{Si} + C_C \rightarrow Si_C + C_{Si}$ | 4.84 |
| $Zr_i + V_{Al} \rightarrow Zr_{Al}$ | -1.72 | $Zr_i + V_{Si} \rightarrow Zr_{Si}$ | −1.57 |
| $C_i + V_{Al} \rightarrow C_{Al}$ | 0.46 | $C_i + V_{Si} \rightarrow C_{Si}$ | 0.42 |
| $Zr_i + Al_{Al} \rightarrow Zr_{Al} + Al_i$ | -0.27 | $Zr_i + Si_{Si} \rightarrow Zr_{Si} + Si_i$ | −0.17 |

## 4 | CONCLUSIONS

This study has considered the powder synthesis of $Zr_3(Al_{1-x}Si_x)C_2$ MAX phases. It is determined here that $Zr_3(Al_{1-x}Si_x)C_2$ forms, with some O contamination therefore producing $Zr_3(Al_{1-x}Si_x)(C_{1-y}O_y)_2$ (with $0 \leq y \leq 0.5$ and with x up to about 0.1). Furthermore, the characterization of the obtained powders and comparison with analogous work[10] suggest that the key for $Zr_3AlC_2$ and $Zr_3(Al_{1-x}Si_x)C_2$ successful synthesis is to surpass the nucleation free energy barrier without favoring competitive phase formation. This was presumably achieved here and in the Lapauw et al.[10] study owing to a heterogeneous MAX phase nucleation process occurring at the surface of $Zr_ySi_z$ phase(s). Maximum yield reported in this study is 59 wt%, which is the same yield reported by Lapauw et al.[10] for $Zr_3AlC_2$. As Si additions to $Ti_3AlC_2$ powder reaction mixes had already proven to ameliorate the quality of the produced compound,[19-21] it is envisaged that Si impurities or deliberate additions could by such mechanisms help in forming or improving the quality of several other MAX phases. The formation of $Zr_3(Al_{1-x}Si_x)C_2$ is a significant extension of the MAX phase family and should be further investigated experimentally in view of its potential nuclear applications.

A preliminary investigation of the radiation resistance of some $M_3AX_2$ phases (M=Zr or Ti; A=Al or Si, and X=C) was conducted. For the $Zr_3AlC_2$ and $Zr_3SiC_2$ MAX phases considered the dominant intrinsic disorder mechanism was calculated to be the Frenkel reaction (relation 2). Its higher energy for $Zr_3AlC_2$ implies its better radiation tolerance. The even higher energy for $Ti_3AlC_2$ implies it will be an even better material in a radiation environment, however, $Zr_3AlC_2$ may be more compatible in a Zr-based alloy nuclear fuel cladding system. Moreover, $Zr_3AlC_2$ is a hard-to synthesize material and success with $Zr_3AlC_2$ coatings for Zr-based alloys for nuclear fuel cladding systems would depend on the possibility of producing coatings by CVD or PVD, which is far from the purpose of this study.

Finally, here we have concentrated on the defect reaction mechanisms but not on the impact of the concentration of point defects on the lattice stability. This will influence the propensity of the material to amorphize in a radiation environment. The other issue that needs to be investigated is the kinetics of the processes: that is, the migration energy barriers for point defects such as interstitials and vacancies to diffuse and annihilate harmlessly by recombination in a process that is reverse to the Frenkel reactions.

## FILES REPOSITORY

XRD raw data supporting this study can be found in Zenodo at https://doi.org/10.5281/zenodo.264285 and is openly available under a CC-BY license.

## REFERENCES

1. Nowotny H. Strukturchemie einiger verbindungen der ubergangsmetalle mit den elementen C, Si, Ge, S. *Prog Solid State Chem*. 1970;2:27–70.
2. Barsoum MW, Radovic M. Elastic and mechanical properties of the MAX Phases. *Annu Rev Mater Res*. 2011;41:195–227.
3. Barsoum MW. *MAX Phases: Properties of Machinable Ternary Carbides and Nitrides*. Weinheim, Germany: Wiley-VCH; 2013.
4. Naguib M, Bentzel G, Shah J, Barsoum M. New solid solution MAX phases: $(Ti_{0.5}, V_{0.5})_3AlC_2$, $(Nb_{0.5}, V_{0.5})_2AlC$, $(Nb_{0.5}, V_{0.5})_4AlC_3$ and $(Nb_{0.8}, Zr_{0.2})_2AlC$. *Mater Res Lett*. 2014;2:233–240.
5. Horlait D, Grasso S, Chroneos A, Lee WE. Attempts to synthesise quaternary MAX phases (Zr, M)$_2$AlC and $Zr_2(Al, A)C$ as a way to approach $Zr_2AlC$. *Mater Res Lett*. 2016;4:137.
6. Lapauw T, Lambrinou K, Cabioc'h T, et al. Synthesis of the new MAX phase $Zr_2AlC$. *J Eur Ceram Soc*. 2016;36:1847–1853.
7. Barsoum MW, Brodkin D, El-Raghy T. Layered machinable ceramics for high temperature applications. *Scr Metall Mater*. 1997;36:535–541.
8. Barsoum MW, Yaroschuck BG, Tyagi S. Fabrication and characterization of $M_2SnC$ (M=Ti, Zr, Hf and Nb). *Scr Metall Mater*. 1997;37:1583–1591.
9. Hu C, Zhang H, Li F, Huang Q, Bao Y. New phases' discovery in MAX family. *Int J Refract Met Hard Mater*. 2013;36:300–312.
10. Lapauw T, Halim J, Lu J, et al. Synthesis of the novel $Zr_3AlC_2$ MAX phase. *J Eur Ceram Soc*. 2016;36:943–947.
11. Middleburgh SC, Lumpkin GR, Riley D. Accommodation, accumulation, and migration of defects in $Ti_3SiC_2$ and $Ti_3AlC_2$ MAX phases. *J Am Ceram Soc*. 2013;96:3196–3201.
12. Horlait D, Grasso S, Al Nasiri N, Burr PA, Lee WE. Synthesis and high-temperature oxidation of MAX phases in the Cr-Ti-Al-C quaternary system. *J Am Ceram Soc*. 2016;99:682–690.
13. Cabioc'h T, Eklund P, Mauchamp V, Jaouen M, Barsoum MW. Tailoring of the thermal expansions of the MAX phases in the $Cr_2(Al_{1-x}, Ge_x)C_2$ system. *J Eur Ceram Soc*. 2013;33:897–904.
14. Ingason AS, Dahlqvist M, Rosen J. Magnetic MAX phases from theory and experiments; a review. *J Phys Condens Matter*. 2016;28:433003.
15. Nechiche M, Gauthier-Brunet V, Mauchamp V, et al. Synthesis and characterization of a new $(Ti_{1-\varepsilon}, Cu_\varepsilon)_3(Al, Cu)C_2$ MAX phase solid solution. *J Eur Ceram Soc*. 2017;37:459–466.
16. Horlait D, Middleburgh SC, Chroneos A, Lee WE. Synthesis and DFT investigation of new bismuth-containing MAX phases. *Sci Rep*. 2016;6:18829.
17. Bragg-Sitton S. Development of advanced accident tolerant fuels for commercial LWRs. *Nucl News*. 2014;March:83–91.
18. Xu P, Lahoda EJ. inventor; Westinghouse Electric Company Llc, assignee. High Temperature Strength, Corrosion Resistant,

Accident Tolerant Nuclear Fuel Assembly Grid. United States patent US20150098546 A1. 2015 Apr 9.

19. Xu X, Ngai TG, Li Y. Synthesis and characterization of quaternary $Ti_3Si_{(1-x)}Al_xC_2$ MAX phase materials. *Ceram Int*. 2015;41:7626–7631.

20. Zhu J, Mei B, Xu X, Liu J. Synthesis of single-phase polycrystalline $Ti_3SiC_2$ and $Ti_3AlC_2$ by hot pressing with the assistance of metallic Al or Si. *Mater Lett*. 2004;58:588–592.

21. Zhou W, Mei B, Zhou J. Fabrication of high-purity ternary carbide $Ti_3AlC_2$ by spark plasma sintering technique. *Ceram Int*. 2007;33:1399–1402.

22. Chen JX, Zhou YC. Effect of SI content on the oxidation resistance of $Ti_3Al_{1-x}Si_xC_2$ (x≤0.25) solid solutions at 1000–1400°C in air. *Oxid Met*. 2006;65:123–135.

23. Gao H, Benitez R, Son W, Arroyave R, Radovic M. Structural, physical and mechanical properties of $Ti_3(Al_{1-x}Si_x)C_2$ solid solution with x=0–1. *Mat Sci Eng A*. 2016;676:197–208.

24. Arroyave R, Talapatra A, Duong T, Son W, Gao H, Radovic M. Does aluminium play well with others? intrinsic Al-A alloying behaviour in 211/312 MAX phases. *Mater Res Lett*. 2016;. doi:10.1080/21663831.2016.1241319.

25. Roisnel T, Rodriguez-Carvajal J. WinPLOTR: a window tool for powder diffraction patterns analysis. *Mater Sci Forum*. 2001;378:118–123.

26. Payne MC, Teter MP, Allan DC, Arias TA, Joannopoulos JD. Iterative minimization techniques for ab initio total-energy calculations: molecular dynamics and conjugate gradients. *Rev Mod Phys*. 1992;64:1045.

27. Segall MD, Lindall PJD, Probert MJ, et al. First-principles simulation: ideas, illustrations and the CASTEP code. *J Phys Condens Matter*. 2002;14:2717.

28. Perdew J, Burke K, Ernzerhof M. Generalized gradient approximation made simple. *Phys Rev Lett*. 1996;77:3865.

29. Vanderbilt D. Soft self-consistent pseudopotentials in a generalized eigenvalue formalism. *Phys Rev B*. 1990;41:7892.

30. Monkhorst HJ, Pack JD. Special points for Brillouin-zone integrations. *Phys Rev B*. 1976;13:5188.

31. Jackson H, Lee WE. Properties and characteristics of ZrC. *Compr Nucl Mater*. 2012;2:339–372.

32. Iwata T, Hattori E, Sugiura K, Hashimoto S, Nakano H, Fukuda K. Syntheses and crystal structures of Si-bearing layered carbides $ZrAl_8C_7$ and $ZrAl_4C_4$. *J Ceram Soc Jpn*. 2009;117:37–41.

33. Sugiura K, Iwata T, Yoshida H, Hashimoto S, Fukuda K. Syntheses, crystal structures and Si solubilities of new layered carbides $Zr_2Al_4C_5$ and $Zr_3Al_4C_6$. *J Solid State Chem*. 2008;181:2864–2868.

34. Dahlqvist M, Alling B, Abrikosov IA, Rosen J. Phase stability of $Ti_2AlC$ upon oxygen incorporation: a first-principles investigation. *Phys Rev B*. 2010;81:024111.

35. Mockute A, Dahlqvist M, Hultman L, Persson PO, Rosen J. Oxygen incorporation in $Ti_2AlC$ thin films studied by electron energy loss spectroscopy and ab initio calculations. *J Mater Sci*. 2013;48:3686.

36. Persson PO, Rosen J, McKenzie DR, Bilek MMM. Formation of the MAX-phase oxycarbide $Ti_2AlC_{1-x}O_x$ studied via electron energy-loss spectroscopy and first-principles calculations. *Phys Rev B*. 2009;80:092102.

37. Rosen J, Persson POA, Ionescu M, Kondyurin A, Mckenzie DR, Bilek MMM. Oxygen incorporation in $Ti_2AlC$ thin films. *Appl Phys Lett*. 2008;92:064102.

38. Dahlqvist M. Benefits of oxygen incorporation in atomic laminates. *J Phys Condens Matter*. 2016;28:135501.

39. Baben M, Shang L, Emmerlich J, Schneider JM. Oxygen incorporation in $M_2AlC$ (M=Ti, V, Cr). *Acta Mater*. 2012;60:4810.

40. Prescott CH. The equilibrium between zirconium oxide and carbon and their reaction products at incandescent temperatures. *J Am Chem Soc*. 1924;48:2534–2550.

41. Zapata-Solvas E, Jayaseelan DD, Brown PM, Lee WE. Effect of $La_2O_3$ addition on long-term oxidation kinetics of $ZrB_2$-SiC and $HfB_2$-SiC ultra-high temperature ceramics. *J Eur Ceram Soc*. 2014;34:3535–3548.

42. Sear RP. Nucleation: theory and applications to protein solutions and colloidal suspensions. *J Phys Condens Matter*. 2007;19:033101.

43. Gibson JB, Goland AN, Milgram M, Vineyard GH. Dynamics of radiation damage. *Phys Rev*. 1960;120:1229.

44. Sickafus KE, Minervini L, Grimes RW, et al. Radiation tolerance of complex oxides. *Science*. 2000;289:748–751.

45. Kröger FA, Vink HJ. Relations between the concentrations of imperfections in crystalline solids. *Solid State Phys*. 1956;3:307–435.

46. Voskoboinikov RE, Lumpkin GR, Middleburgh SC. Preferential formation of Al self-interstitial defects in γ-TiAl under irradiation. *Intermetallics*. 2013;32:230–232.

47. Weber WJ. Radiation-induced swelling and amorphization in $Ca_2Nd_8(SiO_4)_6O_2$. *Radiat Eff*. 1983;77:295–308.

48. Clinard Jr FW , Rohr DL, Roof RB. Structural damage in a self-irradiated zirconolite-based ceramic. *Nucl Instrum Methods Phys Res B*. 1984;1:581–586.

49. Whittle KR, Blackford MG, Aughterson RD, et al. Radiation tolerance of $M_{n+1}AX_n$ phases, $Ti_3AlC_2$ and $Ti_3SiC_2$. *Acta Mater*. 2010;58:4362–4368.

50. Liu XM, Le Flem M, Bechade JL, Monnet I. Nanoindentation investigation of heavy ion irradiated $Ti_3(Si, Al)C_2$. *J Nucl Mater*. 2010;401:149–153.

51. Liao T, Wang JY, Li MS, Zhou YC. First principles study of oxygen incorporation and migration mechanism in $Ti_2AlC$. *J Mater Res*. 2009;24:3190.

52. Wang JM, Liu B, Wang JY, Zhou YC. Theoretical investigation of thermodynamic stability and mobility of the intrinsic point defects in $Ti_3AC_2$ (A=Si, Al). *Phys Chem Chem Phys*. 2015;17:8927.

53. Liu B, Petersen B, Zhang YW, Wang JY, Weber WJ. Layered structure induced anisotropic low energy recoils in $Ti_3SiC_2$. *J Am Ceram Soc*. 2016;99:2693.

54. Zhang HB, Wang JM, Wang JY, Zhou YC, Peng SM, Long XG. Role of nanolaminated crystal structure on the radiation damage tolerance of $Ti_3SiC_2$: theoretical investigation of native point defects. *J Nanomater*. 2013;2013:831590.

55. Bugnet M, Mauchamp V, Eklund P, Jaouen M, Cabioc'h T. Contribution of core-loss fine structures to the characterization of ion irradiation damages in the nanolaminated ceramic $Ti_3AlC_2$. *Acta Mater*. 2013;61:7348.

56. Liu XM, Le Flem M, Bechade JL, Onimus F, Cozzika T, Monnet I. XRD investigation of ion irradiated Ti3Si0.90Al0.10C2. *Nucl Instrum Method Phys Res B*. 2010;268:506–512.